IEEE Open Journal of
Circuits and Systems

Received 8 December 2025; revised 30 January 2026; accepted 5 February 2026. Date of publication 12 February 2026; date of current version 4 March 2026.

Digital Object Identifier 10.1109/OJCAS.2026.3664175

A Miniaturized Ingestible Capsule With Integrated ASIC for Energy-Efficient Sensing in the Gastrointestinal Tract

RAMZY RAMMOUZ[1], VASILEIOS ADAMOPOULOS[1], IVAN D. CASTRO MILLER[1], WIM SIJBERS[1], RIA SIJABAT[2,3], DIMITRIOS FIRFILIONIS[2,3], QIUYANG LIN[1] (Member, IEEE), BENJAMIN CALMÉ[4] (Member, IEEE), AND TOM TORFS[1]

[1]imec Leuven, 3001 Leuven, Belgium
[2]OnePlanet Research Center, 6708 Wageningen, The Netherlands
[3]imec, 6708 Wageningen, The Netherlands
[4]STORM Lab, Institute of Autonomous Systems and Sensing (IRASS), School of Electronic and Electrical Engineering, University of Leeds, LS2 9JT Leeds, U.K.

This article was recommended by Associate Editor S. Shah.

CORRESPONDING AUTHOR: R. RAMMOUZ (ramzy.rammouz@imec.be)

This work was supported by European Commission through the Horizon 2020 Program, under Grant Agreement (GA) AUTOCAPSULE under Contract 952118.

ABSTRACT Recent efforts have focused on wireless ingestible sensing capsules, but challenges remain in miniaturization, sensor integration, and energy efficiency. This paper presents GISMO-A, an ingestible capsule integrating a custom-designed application-specific integrated circuit (ASIC) for low-power biochemical sensing. The ASIC enables pH and oxidation-reduction potential (ORP) measurements at an average power consumption of 172 μW, representing a 70% reduction compared to the previously published GISMO capsule. GISMO-A supports a 6-second measurement interval, resulting in a threefold increase in data density relative to GISMO. Validated through in-vitro and in-vivo experiments, GISMO-A represents a significant advancement in the design of energy-efficient, miniaturized GI Tract sensing systems.

INDEX TERMS Application specific integrated circuit, biochemical sensing, low-power, gastrointestinal tract, ingestible capsule, miniaturized, temporal resolution.

I. INTRODUCTION

THE gastrointestinal (GI) tract plays a vital role in maintaining overall health, influencing digestion, immune function, and nutrient absorption. Disruptions in its function are often associated with a wide range of conditions, including chronic inflammatory diseases, metabolic disorders, and infections. As such, monitoring the GI tract is essential for health management and disease diagnosis [1]. Conventional diagnostic methods, such as endoscopy, are inherently invasive and typically limited to punctual assessments. These procedures often require clinical settings and sedation. They are also unsuitable for capturing dynamic changes in the GI environment over extended periods of time [2].

In contrast, ingestible capsules offer a minimally invasive alternative and collect data as they naturally transit through the digestive system. This enables non-disruptive monitoring under real-life conditions.

Camera-based ingestible capsules such as PillCam [3], Endocapsule [4], and CapsoCam Plus [5] have focused on providing less invasive optical imaging, delivering data for diagnosing structural abnormalities in the GI tract. However, a substantial proportion of GI disorders - particularly functional GI disorders such as irritable bowel syndrome (IBS), motility disorders, and functional dyspepsia - do not present visible abnormalities and are therefore undetectable through imaging alone. These conditions are highly prevalent and account for approximately 40% of gastroenterology consultations in the U.S. according to the International Foundation for Gastrointestinal Disorders [6]. Moreover, visual inspection alone is insufficient for assessing gut health and nutritional status, both of which are essential for a comprehensive understanding of GI health [7].

Recent advances have therefore shifted focus toward wireless ingestible capsules for sensing [8], [9]. Table 1-A gives an overview of relevant devices developed to date, highlighting their sensing capabilities, size, and battery life. Despite offering deeper insights into GI function and pathology, most remain relatively large (often exceeding FDA size 000), have limited integration of multiple sensing modalities, and have limited operational lifespan.

TABLE 1. Overview of ingestible capsules for sensing.

	A. State of the art of ingestible sensing capsules							B. This work	
	Smart Pill, 2001 [10], [11]	Atmo gas sensing capsule, 2018 [12]	Gopalakri-shnan, 2023 [13]	Inda-Webb, 2023 [14]	PillTrek 2025 [15]	Yang 2025 [16]	GISMO, 2025 [17]	GISMO-A-Primary	GISMO-A-Rechargeable
Diameter (mm)	11.7	11	11	14.3	7	11	7.5	7.5	9.8
Length (mm)	26.8	28	22	8.5	25	29	21	21	25.5
Approx. volume (cm^3)	2.5	2.3	1.7	1.4	~1	2.5	0.8	0.8	1.7
Closest FDA Size	> size 000	> size 000	> size 000	NA	~ size 00	> size 000	< size 0	< size 0	size 000
Battery Life	> 5 days	3 days	NA	1 month	>22h	NA (Energy harvesting)	5 days [1] (20s interval)	11 days (6s interval)	9 days rechargeable (3 min interval)
Measurement	Motility, pressure, pH, Temp	Gas (H2, O2, CO2, CH4)	pH, ORP	Inflam. biomarkers	pH, serotonin, glucose, ions, Temp	pH for drug delivery	pH, ORP, Temp	pH, ORP, Temp	pH, ORP, Temp
Validation	Human	Human	In-vitro	Pig	In-vitro and rabbits	In-vitro and ex-vivo	Human	Bench (not final encapsulation)	In-vitro and pig

[1] in addition to 9 days in ultra-low-power mode with reduced functionality (only temperature)

GISMO (GastroIntestinal Smart Module) [17] addressed these limitations and is, to our knowledge, the first ingestible sensing capsule developed and validated in humans with a form factor smaller than FDA size 0. It integrates an electrochemical reference electrode along with sensors for pH, oxidation-reduction potential (ORP), and temperature. The device was also successfully validated in human studies. In addition to 5 days of operation in full functionality mode with a temporal measurement resolution of 20 seconds, GISMO ensures 9 additional days of ultra-low-power mode with reduced functionality (only temperature sensing) to detect the excretion of the capsule.

During the development of the GISMO capsule, it was observed that approximately 52% of its total energy consumption was due to biochemical sensor acquisition. This insight highlighted the need to optimize power usage during biochemical sensing as a critical step toward improving overall energy efficiency. To address this challenge, a custom-designed ASIC was integrated into the system to enable low-power biochemical sensing, resulting in the development of GISMO-A.

This paper presents the design of GISMO-A with particular emphasis on the integration of the ASIC. The device's biochemical sensing capabilities are evaluated through both in-vitro and in-vivo experiments. Its power efficiency is demonstrated in a dedicated experimental setup, showing a threefold increase in the number of data points collected compared to the GISMO capsule, using identical batteries.

II. SYSTEM ARCHITECTURE

The proposed system architecture is illustrated in Fig. 1. To enable power-efficient biochemical sensing, GISMO-A integrates the custom-designed ASIC demonstrated in [18] for a different application. This ASIC functions as a highly integrated analog front-end with configurable biasing, specifically tailored for interfacing with biochemical sensors. It enables biasing and digitization of signals from the pH ISFET and ORP sensors that were previously validated in GISMO.

The ASIC is connected to a microcontroller unit (MCU), which is responsible for initiating configuration and measurement commands. However, the ASIC autonomously manages all low-level operations, including sensor biasing, signal settling, and sampling. This allows the MCU to remain in a low-power idle state during these time-consuming processes, significantly reducing overall power consumption. Once the measurement is complete, the MCU retrieves the data.

In addition to biochemical sensing, the system incorporates digital sensors for temperature, acceleration, and magnetic field measurements. All sensors are sampled periodically, and the collected data is transmitted wirelessly to a wearable receiver using an 868 MHz RF transceiver and a conformal antenna.

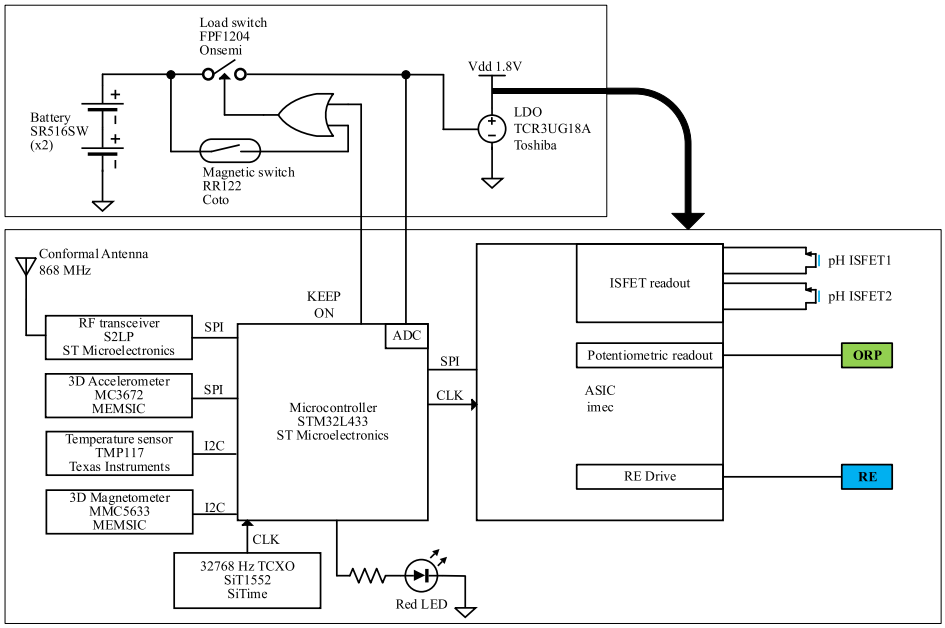

FIGURE 1. Block diagram of GISMO-A.

The electronics are designed to be powered by two SR516 silver oxide coin cell batteries and to fit within a size 0 biocompatible enclosure (21.7 mm long x 7.6 mm diameter), ensuring suitability for ingestible applications.

III. BIOCHEMICAL SENSING ASIC

The multimodal biochemical sensor interface ASIC, previously validated for bioreactor monitoring [18], [19] has been employed in this work. The detailed block diagram is presented in Fig. 2. The design includes two potentiometric channels. The voltage between the Working Electrode (WE) and the Reference Electrode (RE) is measured via two pseudo-differential buffers with ESD protection leakage compensation to minimize input bias current. In addition, the buffer's input pair uses thick-oxide transistors to further reduce leakage. Both buffers are powered by a 3.6 V on-chip charge pump. This arrangement increases the potentiometric channel's voltage headroom while preserving high linearity. The Reference Electrode potential is set by a driver with the desired voltage set up by an 8-bit digital-to-analog converter (DAC).

Additionally, four ISFET channels permit measuring the medium's pH by sensing shifts in the threshold voltage of the ISFET caused by the hydrogen-ion concentration. The liquid gate potential is driven by a driver and an 8-bit DAC. The ISFET readout uses a constant-current, constant-voltage architecture [20], which is commonly used to bias ISFETs in the linear region. The ASIC provides programmable ranges for the drain-source current (10 nA to 100 μA across 13 discrete levels), and the drain-source voltage bias (25 mV to 600 mV across 5 levels). These ranges are chosen to cover the nominal operating conditions of commercial ISFET sensors [21], while extending toward lower current and voltage settings to support lower power biasing.

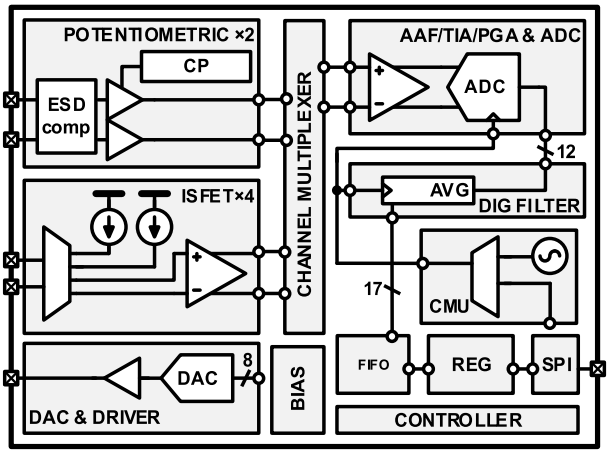

FIGURE 2. Block diagram of the biochemical sensor interface ASIC [18].

All sensing channels are time-multiplexed through a switch matrix into the analog backend, which performs filtering, amplification, and analog-to-digital conversion. Digital control handles register settings, clocking, digital filters, and communication.

Implemented in a 3.2 mm x 3.2 mm Ball Grid Array package, this multimodal biochemical sensor interface ASIC is well-suited for monitoring in the GI tract.

IV. SYSTEM DESIGN

A. ELECTRONIC CIRCUIT

As illustrated in Fig. 1, the circuit integrates a low-power ARM Cortex-M4F microcontroller (STM32L433, STMicroelectronics), which manages system operations and performs AES-128 encryption of the data. The firmware running on the MCU is initially programmed with a connector but can be

upgraded over the wireless 868 MHz RF link after encapsulation, enabling upgrades and bug fixes. The circuit also includes a digital temperature sensor (TMP117, I2C), a 3D magnetometer (MMC5633, I2C) and a 3D accelerometer (MC3672, SPI). Data is transmitted to the wearable device via an 868 MHz transceiver (S2LP, SPI).

To support the biochemical sensing interface ASIC, a 32.768 kHz clock is required. This is provided by a miniature, low-power temperature-controlled oscillator (TCXO, SiT1552, 1 mm x 0.8 mm, <1 μA current consumption), which serves as an external clock source for the MCU. The MCU then forwards this clock signal to the ASIC.

Three biochemical sensing channels are used in the system: two pH ISFETs and one potentiometric (ORP). A single reference electrode (RE) is shared among these channels. The potential of this electrode is driven by the ASIC.

B. ASIC CONFIGURATION

The biochemical sensor channels are measured sequentially in the ASIC using single-shot mode. For each channel, the ASIC sets the biasing conditions, then waits for the settling time before starting to sample on the analog-to-digital converter (ADC). Digitized samples are then averaged in a single output transmitted via SPI to the MCU. The number of averaged samples per measurement could be set between 1 (30 μs sampling time) and 32768 (1 s sampling time). The setting of 2048 averaged samples per measurement (60 ms sampling time) was selected as a trade-off between noise level and power consumption.

The biasing conditions were individually set for each sensor. For ISFETs, measurements were conducted to find the optimal biasing conditions: the Drain-Source Current (IDS) and the Drain-Source Voltage (VDS) while keeping the reference electrode voltage to 1.5 V as for GISMO. This was done considering the current consumption during the ISFET measurement and the target pH range of 1 to 10, accounting for ISFET device variability.

For each biasing condition, the supported pH range was derived from the combined constraints of the ASIC's allowable voltage ranges and the expected range for the ISFET's electrical characteristics regarding sensitivity and offset, as determined by the manufacturer's specifications in combination with an empirical determination of the dependency of these characteristics on the bias conditions. A pH value is considered supported if both VS and VD remain within the ASIC voltage limits.

The total current consumption of the system while biasing and measuring a single ISFET was measured, in order to quantify the impact of the biasing conditions on the overall energy consumption.

Based on the results in table 2, 10 μA IDS and 100 mV VDS were selected as they ensured the lowest current consumption and supported pH values from 1 to 10.

For the ORP sensor, the reference electrode voltage was set to 1V, allowing an input range of -900mV to +600mV. The settling time – defined as the delay between applying the bias conditions and initiating ADC sampling – was set to 500 ms for all sensors.

TABLE 2. Comparison between different ISFET biasing conditions.

ISFET biasing conditions (IDS/VDS)	Supported pH range	Total current consumption (µA)
100 µA / 600 mV	4 to 9	172
25 µA / 300 mV	3 to 10	45
25 µA / 100 mV	0 to 10	45
10 µA / 300 mV	4 to 10	33
10 µA / 100 mV	1 to 10	33

C. PCB IMPLEMENTATION

An assembly of 3 stacked miniature PCBs is used. Fig. 3 shows how functionality is divided among the 3 PCBs. Rigid PCB 1 is a 600-μm-thick, 6-layer high-density interconnect 5.8 mm $\times$ 10.8 mm PCB, while rigid PCB 2 is a 400-μm, 4-layer PCB of the same size. The sensor PCB is implemented on a 150-μm-thick two-layer polyimide flexible PCB. Fig. 4 shows the stack of PCB 1 and PCB 2 and highlights the ASIC in orange.

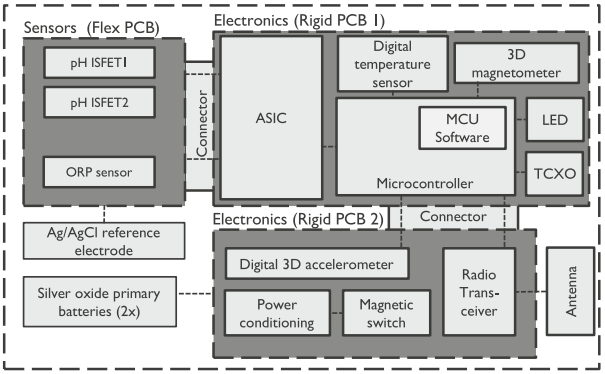

FIGURE 3. Block diagram of the PCBs in the capsule.

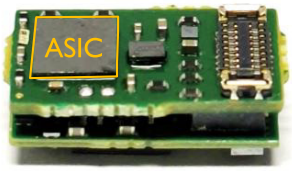

FIGURE 4. Stack of rigid PCBs 1 and 2.

D. CAPSULE ASSEMBLY

Fig. 5 shows GISMO-A's building blocks for a size 0 capsule (length 21 mm, diameter 7.5 mm) with disposable 2xSR516SW batteries (5.8 mm diameter, nominal capacity 12.5 mAh). This capsule, GISMO-A-Primary, when fully assembled, would occupy the same volume as GISMO. Its PEEK housing, reference electrode and sensor flex are identical to those used in GISMO, for which the biocompatibility was previously assessed [17].

For this initial prototype, the possibility of performing multiple over-the-air firmware upgrades to the device is needed. Therefore, the device is built in wired (GISMO-A-Wired) and rechargeable (GISMO-A-Rechargeable) variants to ensure such firmware upgrades do not impact battery life and subsequent validation. The wired variant uses externally connected batteries while the rechargeable integrates a rechargeable coin cell battery MS621 (6.8 mm diameter, 5.5 mAh nominal capacity).

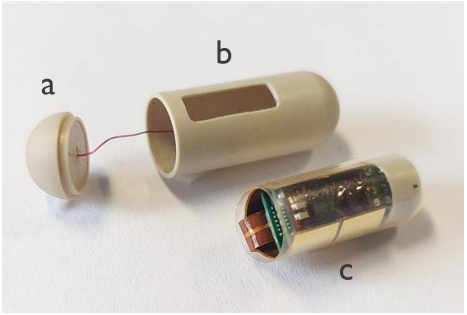

FIGURE 5. Building blocks for GISMO-A-Primary (size 0): (a) the housing of the reference, (b) the body of the capsule(PEEK), (c) the electronics (PCBs, antenna and batteries) in a size 0 gelatine capsule.

(a) (b)

FIGURE 6. Built variants of GISMO-A: GISMO-A-Rechargeable (a) and GISMO-A-Wired (b).

Both variants are built in-house in a similar way to GISMO, but in the larger size 000 capsules (length 25.5 mm; diameter 9.8 mm). This increase in volume ensured the rechargeable battery (for the rechargeable variant) and the supply wires (for the wired variant) fit in the encapsulation. Both variants are shown in Fig. 6.

V. EXPERIMENTAL VALIDATION

Multiple experiments were conducted to validate the operation of the proposed device. These experiments focused on biochemical sensing functionality and battery life.

A. VALIDATION OF THE ENCAPSULATION

The first step of the experimental validation was performed on GISMO-A-Rechargeable labelled ID#34. It aimed to validate the assembly, particularly the hermeticity of the enclosure.

Submerged in a pH 7 buffer solution at room temperature, ID#34 was configured to transmit a measurement every 3 minutes. This rate was selected to ensure an operation time of 9 days with the rechargeable MS621 battery, exceeding the longest time in the body reported in [17] which was 7.41 days.

During this experiment, ID#34 remained operational for 10 days and 15.5 hours. As shown in Fig. 7 - "Initial test", the measured potential for both pH ISFETs is stable throughout this experiment, with the average values of measured potential for pH ISFET 1 and pH ISFET 2 at 908 $\pm$1.25 mV and 982 $\pm$1.01 mV, respectively. These observations are consistent with the absence of any ingress and that the encapsulation meets the hermeticity requirement, considering that, based on the capsule's design and previous experience in [17], any ingress that would have reached any part of the electronic circuitry would be expected to affect the operational lifetime and/or the stability of the sensor signals.

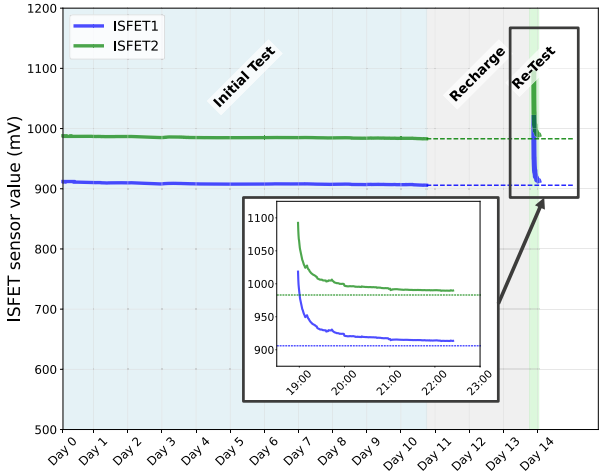

FIGURE 7. Measured potential on pH ISFETs during the experiment for the validation of the encapsulation.

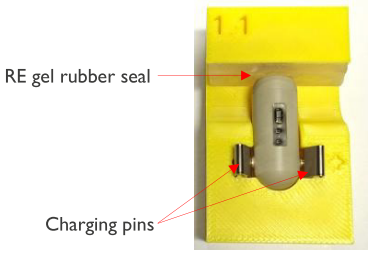

FIGURE 8. Holder used to store and recharge GISMO_A_Rechargeable.

After recharging ID#34, a stabilization effect, as shown in Fig. 7 – "Re-test", was observed on the biochemical sensors. Directly after submersion, all biochemical sensors output higher values. These values then drop progressively and converge to the ones measured in the initial experiment. This observation is consistent with the hypothesis of the reference electrode gel drying during the recharging. This could possibly be due to the 3D-printed holder used to store and to recharge the device (shown in Fig. 8). The variation in the mechanical dimensions of the 3D-printed holder due to the printer tolerance may have resulted in suboptimal sealing of the reference electrode gel on some holders. Since GISMO-A-Rechargeable and GISMO-A-Wired variants will

only be used in this initial prototype, this issue can be prevented on the size 0 GISMO-A-Primary capsules by storing them in a milled holder with improved manufacturing tolerances, as was done for the GISMO capsules.

To work around this stabilization time issue, for the following experiments, ID#34 was submerged in the liquid until stabilization of the sensor's output: Data is recorded after that point.

B. IN-VITRO VALIDATION OF BIOCHEMICAL SENSORS

This test aims to validate the operation of the capsule's biochemical sensors in GI simulated fluids with different pH values over a long period. For this purpose, ID#34 was attached to a 3D printed holder and submerged in different reference solutions. The experimental setup is shown in Fig. 9 while the detailed experimental procedure is described in Table 3. All parts of the experiment were conducted in a temperature-controlled water bath at 37 °C to emulate physiological conditions.

The intermittent calibration (CAL) at 48h, 6 days and 8 days was done to confirm the sensors' specifications. We followed the same calibration procedure and acceptance criteria in [17] to evaluate the sensors in ID#34. The device was sequentially submerged in four pH standards (pH 2, 4, 7 and 9; Avantor 20 °C AVS TITRINORM; accuracy ±0.02 pH units) then in an ORP +220 mV standard (51350060, 220 mV/pH 7, Mettler Toledo; 180–220 mV at 37 °C).

The biochemical sensor data wirelessly transmitted to the receiver by the ID#34 were recorded and post-processed. The slope and the offset of the pH ISFET are then calculated based on the measured value in millivolts in the four pH solutions. An ISFET sensor is labelled in-spec if its slope is between -49 mV/pH and -56 mV/pH.

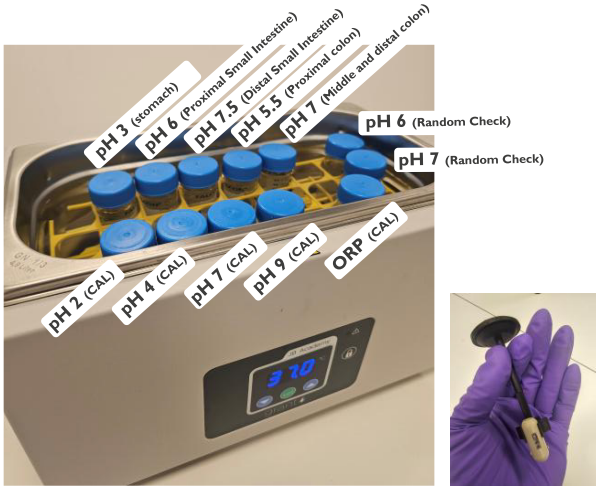

FIGURE 9. Experimental setup for the in-vitro validation of biochemical sensors.

The verification of the ORP sensor is a one-point verification: the sensor is labelled in-spec if its output in the +220 mV standard solution is between 180 mV and 220 mV.

TABLE 3. Experimental procedure for the in-vitro validation of the biochemical sensors.

Start time	Duration	Reference solutions at 37deg. C
0d0h	1h	pH 3 (to mimic the stomach)
0d1h	16h	pH 6 (to mimic the proximal part of the small intestine)
0d17h	4h	pH 7.5 (to mimic the distal part of the small intestine)
0d21h	4h	pH 5.5 (to mimic the cecum/proximal colon)
1d1h (25h)	23h	pH 7 (to mimic the large intestine (middle and distal colon))
2d (48h)	2.5h	Calibration using pH 2, 4, 7, 9 calibration solution and ORP 220 mV standard solution (0.5h in each solution)
2d2.5h	3d21.5h	pH 7 (random check)
6d	2.5h	Calibration using pH 2, 4, 7, 9 calibration solution and ORP 220 mV standard solution (0.5h in each solution)
6d2.5h	1d21.5h	pH 6 (random check)
8d	2.5h	Calibration using pH 2, 4, 7, 9 calibration solution and ORP 220 mV standard solution (0.5h in each solution)

As shown in Table 4, the calibration profiles of pH ISFETs and ORP sensors are within the acceptance criteria. This calibration was the only verification done on the ORP sensor during the experiment.

It is important to note that the device was immersed in liquid for a total of 19 days, including the immersion in pH 7 at room temperature during the initial validation for the encapsulation. Using the data from the calibration at 48h, the pH ISFET measurements (in millivolt) were converted to pH values and compared to the output of the commercial pH Horiba sensor. Fig. 10 shows that the pH ISFETs are stable for an 8-day operation time after recharging, in addition to 11 days before recharging. Their profiles matched those of the commercial pH Horiba sensor. The drift observed after 19 total days of immersion in liquids (pH 6, day 7 of the experiment) is 0.32 pH units (17.2 mV) and 0.29 pH units (15.5 mV) respectively for ISFET1 and ISFET2. This is consistent with our previous characterization of the GISMO reference electrode in [17], where we measured an average drift of 0.042 ± 0.012 mV·h^{-1} in a 14-day study done over 10 reference electrodes. The distribution of the Absolute Error is shown in Fig. 11. The Mean Absolute Error (MAE) on pH values of ISFET1 and ISFET2 was 0.181 ± 0.109 pH units and 0.176 ± 0.102 pH units, respectively, compared to the Horiba sensor.

Regarding the ORP sensor, the different calibrations showed it remained within specification until the conclusion of the experiment, except for a small temporary excursion of +1.4 mV beyond the 180 mV to 220 mV specification range at the 6 days calibration.

C. CHARACTERIZATION OF MULTIPLE DEVICES

Seven additional devices (5 GISMO-A-Rechargeable and 2 GISMO-A-Wired) were built, and biochemical sensors were calibrated and then evaluated based on the acceptance criteria.

TABLE 4. ID#34 calibration data during the in-vitro validation of biochemical sensors at 37 °C.

		CAL 48h	CAL 6d	CAL 8d
ISFET1	Slope (mV/pH.U)	-53.5	-53.3	-53.8
	Offset (mV)	1296.1	1289.6	1287.0
ISFET2	Slope (mV/pH.U)	-53.3	-53.0	-53.4
	Offset (mV)	1371.9	1366.0	1363.1
ORP	Value (mV) in 220mV calibration liquid	214.0	221.4	212.6

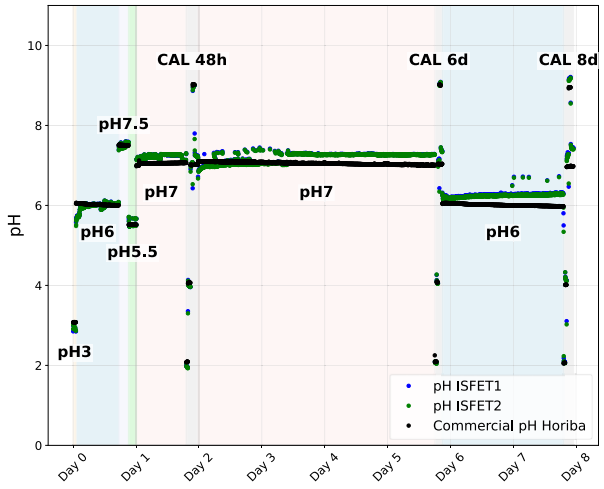

FIGURE 10. Comparison between pH measurements in ID#34 and in the commercial Horiba pH sensor.

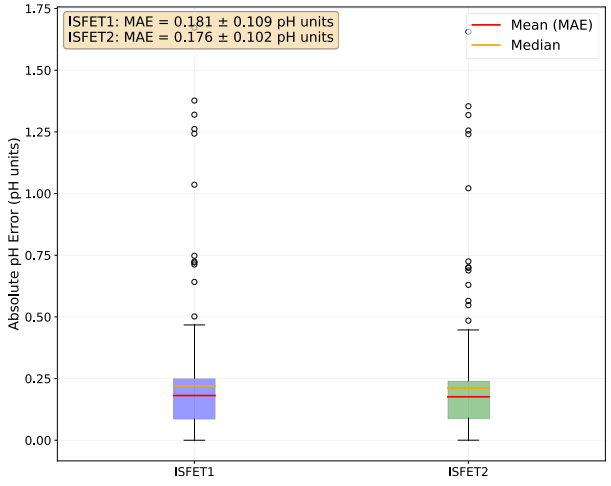

FIGURE 11. Distribution of the pH Absolute Error between ISFETs in ID#34 and the commercial Horiba sensor.

As listed in Table 5, 5 devices have both pH ISFETs within acceptance criteria and all 7 devices have at least 1 pH ISFET in-spec. For the ORP sensor, 4 devices are within the acceptance criteria. Two devices (ID#26 and ID#31) have ORP values of 178.9 mV and 177.9 mV respectively in the 220 mV standard solution: this is slightly below the lower limit of the acceptance criteria (180 mV). One device (ID#30) has a failed ORP sensor, which measured negative ORP values (-29.9 mV) in the expected 180-220 mV ORP solution. Out of 7 devices, ID#21 has the best slope (sensitivity) for both pH ISFETs and a good ORP sensor: this device was selected for the in-vivo validation.

D. IN-VIVO VALIDATION

The biochemical sensors (pH and ORP) integrated into the system have already been extensively validated using the GISMO ingestible platform [17]. While the electronic implementation in GISMO-A differs from that of GISMO, the sensors and sensing principles remain unchanged. This allows the in-vivo validation of GISMO-A to focus on assessing the overall functionality of the device in a live animal model.

The in-vivo experiments (Leeds, UK, May 2025) were conducted within the framework of the AUTOCAPSULE project, in collaboration with the University of Leeds. The validation of GISMO-A was integrated into an already scheduled in-vivo experiment, ensuring that no additional animal subjects were included for the purpose of this validation.

TABLE 5. Data from the first calibration of 5 rechargeable and 2 wired GISMO-A devices.

Variant	ID	pH ISFET			ORP
		Sensor	Slope	Offset	Value (ORP standard)
Rechargeable	21	ISFET1	-54.7	1443.8	199.9
		ISFET2	-54.7	1261.3	
	25	ISFET1	-51.7	1355.7	215.4
		ISFET2	-46.2	1394.6	
	26	ISFET1	-50.4	1340.6	178.9
		ISFET2	-48.9	1199.2	
	30	ISFET1	-52.5	985.8	-29.9
		ISFET2	-53.1	904.6	
	31	ISFET1	-49.3	1252.1	177.9
		ISFET2	-49.0	1389.6	
Wired	24	ISFET1	-53.9	1280.9	208.9
		ISFET2	-53.0	1288.1	
	33	ISFET1	-50.4	1347.2	198.0
		ISFET2	-50.0	1415.6	

This animal work was performed in accordance with the Animals (Scientific Procedures) Act 1986 under project license PP3093153. The protocol was designed, and the trial was performed in-line with the National Centre for the Replacement, Refinement & Reduction of Animals in Research (NC3Rs) and to ensure minimal suffering of the animal. This includes oversight by the University of Leeds facility's veterinary team.

For this procedure, GISMO-A-Rechargeable (ID#21) was attached to an endoscope (Olympus EVIS EXERA II) and introduced into the colon of a fasted, sedated pig (Yorkshire-Landrace gilt, 33 Kg) via the rectal route. The receiver electronics were placed on an acrylic arch-shaped structure mounted around the pig's belly. This emulates a wearable receiver by placing the receiver in proximity to the pig. Fig. 12 is a photo of the experimental setup.

ID#21 was inserted to depths of 10 cm, 20 cm and 30 cm. For each position, data was recorded for 4 mins at the rate of one measurement point every 10 seconds. Measurements were collected by the receiver through the 868 MHz link and sent to a laptop via USB.

Fig. 13 presents the biochemical measurements collected from ID#21 across two experimental iterations. To facilitate comparison, the x-axis in both graphs was scaled to ensure equal distribution of measurements across the three insertion depths. This normalization enables clearer visualization of sensor output at each depth, independent of the number of data points collected per segment. For pH, the displayed value corresponds to the average of the two ISFET sensor readings.

The pH readings are consistent between the two iterations across the different insertion depths, confirming stable sensor performance. For ORP, however, an artefact occurred during the first iteration as ID#21 was repositioned to 20 cm depth. This resulted in significant fluctuations in the ORP signal towards a more oxidative value, which were not settled before the end of the first iteration. This artefact is hypothesized to be caused by the presence of gas over the ORP sensor, resulting in the sensor losing contact with the digesta. This was made more likely by the pig being fasted prior to the experiment. No similar issue was observed in the second iteration, as the output of the sensor was stable across all depths. The ORP values at 10 cm depth – before the artefact – were consistent between both iterations.

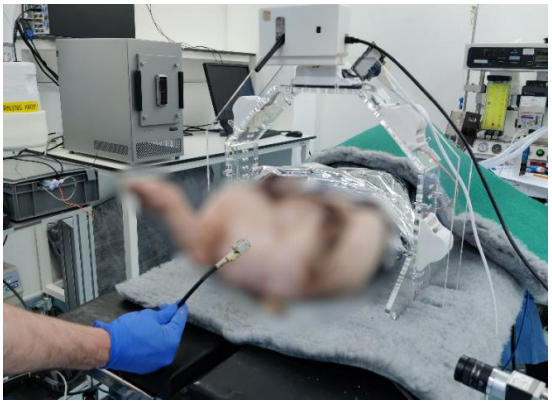

FIGURE 12. Photo of the experimental setup for the in-vivo validation.

Overall, measured pH was consistent with the range of pH 6 to 7 reported in [22] and [23]. ORP values are also consistent with the measurements done on pigs in [17]. Data transmission from inside the body to the outside receiver was also validated: 100% of the samples sent by ID#21 during the experiment were received by the receiver with an average received signal strength of −69 dBm (the receiver can successfully receive signals down to as low as −90 dBm).

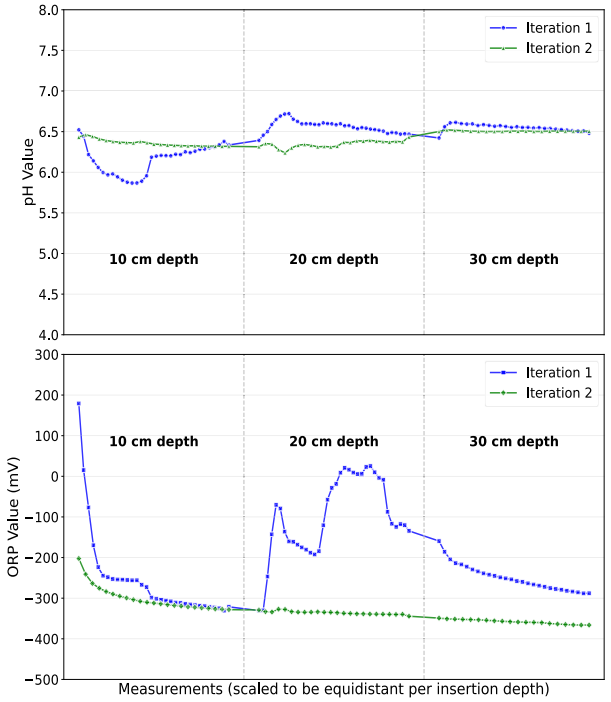

FIGURE 13. ORP and pH as measured by #ID21 in the colon of the pig.

E. VALIDATION OF OPERATION TIME

Since improved power consumption is a key element of the design, current consumption measurements were conducted on GISMO-A-Wired ID#33. Current consumption waveforms were recorded for 100 measurement cycles and then averaged to improve the signal-to-noise ratio for microampere-level currents. Fig. 14-a displays the resulting waveform for a measurement cycle and highlights the operational phases. The waveform shows that the highest current peak occurs during radio transmission (13.5 mA) while the lowest current is recorded when the system is idle (9 μA). On average, GISMO-A consumes 67.5 μA during active phases.

Fig. 14-b shows an annotated zoomed-in view of the current waveform during ISFET2 measurement. The average current consumption during biochemical sensing (2 ISFETs and ORP), including the configuration of the ASIC by the MCU, is 55.6 μA.

Battery discharge experiments were then performed on GISMO-A-Wired ID#33 in non-deionized water at 37 °C, which emulates an in-vivo scenario from an energy consumption perspective. This setup enables evaluation of operational lifetime and energy efficiency of the device by allowing continuous operation until battery depletion, which cannot be reliably achieved in in-vivo studies due to the high variability in transit times for pigs [22]. Supplied with the 2xSR516 batteries intended for GISMO-A-Primary, the device remained operational for 11 days with full functionality, while providing a measurement point every 6 s.

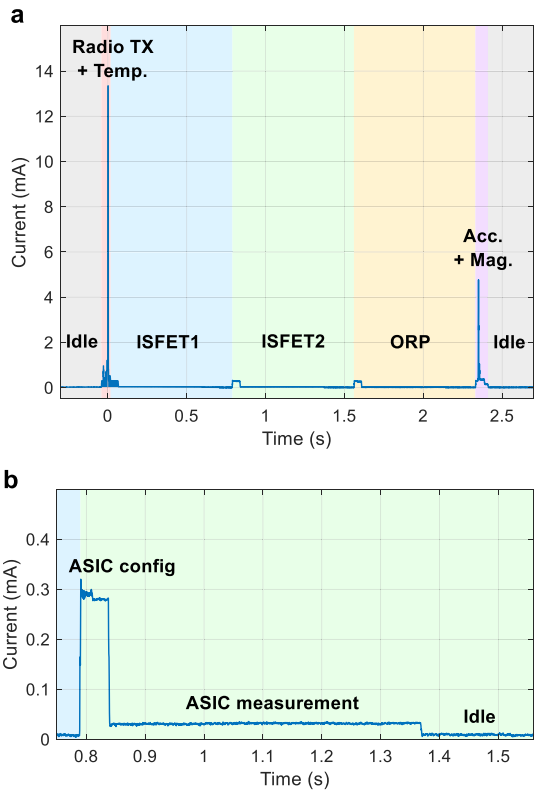

FIGURE 14. Current consumption waveform of GISMO-A during a full measurement cycle (a) and during ISFET2 measurement (b).(Radio TX: Radio transmission, Temp.: Temperature measurement, Acc.: Acceleration measurement, Mag.: Magnetic field measurement).

TABLE 6. Energy repartition per task for GISMO-A capsule with 6 s measurement interval.

Task		Energy percentage	Dominant component
Temperature sensing		7%	STM32L433
Radio transmission		14%	S2LP
Biochemical sensing	ISFET	18%	ASIC
	ORP	7%	ASIC
	ASIC config.	24%	STM32L433
Acceleration and magnetic field sensing		15%	STM32L433 + MMC5633
Idle		14%	All

For this configuration, table 6 shows the energy percentage repartition per task and highlights, for each task, the dominant component. Based on these values, configuring the ASIC by the MCU requires similar energy as performing the measurement in the ASIC itself. This suggests that future optimization should target reducing MCU configuration overhead.

Higher operating times can be reached if the measurement interval is increased. Discharge experiments demonstrated 19 and 42 days of operation time with the sample interval set respectively to 20 s and 5 minutes.

VI. DISCUSSION

Table 1 compares existing ingestible sensing devices (A) to the ones proposed in this work (B). GISMO-A-Primary, together with GISMO, is among the most compact, with a volume of 0.8 cm^3. While this specific form factor was not physically realized, it was demonstrated that the complete system fits within a capsule smaller than FDA size 0, in contrast to most other devices, which exceed size 000.

Even further reductions in the capsule size are mainly limited by the volume of the batteries (SR516SW: 5.8 mm diameter and 1.6 mm height) and the footprint of the PCB stack. Lower power consumption could allow for the use of smaller batteries (e.g. SR416SW 4.8 mm diameter and 1.6 mm in height). However, the current design faces an additional challenge: with the present level of integration, adding new functionalities would likely increase capsule size. Addressing this requires combining functionalities that are currently implemented on separate ICs into application-specific and system-on-chip solutions. For instance, the microcontroller and the radio can be integrated within a single SoC. Other sensing functionalities can likewise be combined into another sensing ASIC by leveraging circuits proposed in the literature, such as the 3D magnetometer in [24] and the temperature sensor in [25].

In terms of power efficiency, this design compares favorably to the GISMO capsule, which, as reported in [17], achieved 5 days of continuous operation at a 20-second measurement interval followed by 9 days in an ultra-low-power mode with reduced functionality. Notably, the biochemical sensing in GISMO-A consumes an average of 172.4 μW (55.6 μA at 3.1 V battery supply), significantly lower than the 565.1 μW (182.3 μA at 3.1 V battery supply) reported for GISMO. This reduction is the most important contributor to the extended operational lifespan.

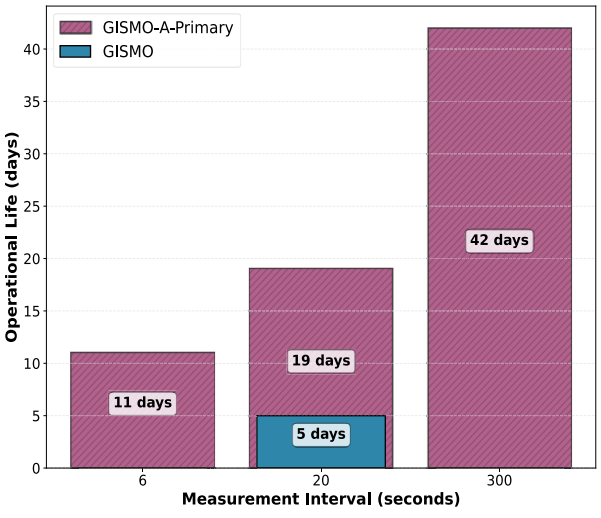

FIGURE 15. Operational life of GISMO-A-Primary compared to GISMO.

Fig. 15 presents a comparative analysis of the operational lifespans of GISMO-A-Primary and GISMO across various measurement intervals. The results indicate that

GISMO-A-Primary enables a 6-second sampling interval for all sensors while maintaining an operational duration 50% higher than the maximum in-body time observed during GISMO's in-human trials. This results in a threefold increase in the number of data points collected. Furthermore, by setting the sampling interval to 20 seconds as in GISMO, the operational life of the capsule in full functionality is 19 days, a four-time increase compared to GISMO.

VII. CONCLUSION

This paper presents the design, implementation, and experimental validation of an ultra-low power ingestible capsule integrating a custom ASIC for energy-efficient biochemical sensing.

The resulting energy surplus opens new possibilities for enhancing data acquisition within the GI tract. Two use cases were demonstrated: (1) reducing the measurement interval to increase data density during typical transit times, and (2) extending operational duration to support longer monitoring periods.

Beyond these improvements, reduced energy consumption could also enable the use of smaller batteries. Coupled with advanced integration through application-specific and system-on-chip solutions, this would allow further miniaturization of devices without compromising functionality.

Moreover, the surplus energy available in GISMO-A opens opportunities for integrating additional sensing modalities or for enabling higher sampling that could provide richer spatiotemporal data and support advanced diagnostic and therapeutic applications [26]. This surplus energy also enables expanding ingestible capabilities by incorporating capsule localization – allowing correlation of measurements with anatomical position, as demonstrated in [27] and [28] – as well as sampling or drug delivery [29]. Future work will explore these directions to further expand the capsule's functionality.

ACKNOWLEDGMENT

The authors would like to thank Alistair Bacchetti, Nikita Greenidge, and Pietro Valdastri for their support during validation.

REFERENCES

[1] J. R. Biesiekierski, C. K. Yao, C. J. Tuck, and M. Snelson, "Methodological advances in gastrointestinal tract physiology measurements: Relevance to nutritional studies," *Proc. Nutrition Soc.*, vol. 84, no. 2, pp. 155–167, May 2025, doi: 10.1017/s0029665124007444.

[2] G. Pan and L. Wang, "Swallowable wireless capsule endoscopy: Progress and technical challenges," *Gastroenterology Res. Pract.*, vol. 2012, pp. 1–9, 2012.

[3] *PillCamTM SB 3 Capsule Endoscopy System*, Medtronic, Minneapolis, USA, 2013.

[4] *ENDOCAPSULE 10*, Olympus, Center Valley, USA, 2014.

[5] *CapsoCam Plus*, CapsoVision, CA, USA, 2016.

[6] International Foundation for Gastrointestinal Disorders. *Functional GI Disorders*. Accessed: Jan. 30, 2026. [Online]. Available: https://iffgd.org/gi-disorders/functional-gi-disorders/

[7] N. Van Helleputte et al., "Miniaturized electronic circuit design challenges for ingestible devices," *J. Microelectromech. Syst.*, vol. 29, no. 5, pp. 645–652, Oct. 2020.

[8] C. Zhang et al., "Ingestible electronic capsules for in situ sensing of diverse biomarkers," *Device*, vol. 3, no. 11, Nov. 2025, Art. no. 100935.

[9] A. Abdigazy, M. Arfan, G. Lazzi, C. Sideris, A. Abramson, and Y. Khan, "End-to-end design of ingestible electronics," *Nature Electron.*, vol. 7, no. 2, pp. 102–118, Feb. 2024.

[10] D. Timm, H. Willis, W. Thomas, L. Sanders, T. Boileau, and J. Slavin, "The use of a wireless motility device (SmartPill) for the measurement of gastrointestinal transit time after a dietary fibre intervention," *Brit. J. Nutrition*, vol. 105, no. 9, pp. 1337–1342, May 2011.

[11] A. Soucasse, A. Jourdan, L. Edin, E. Meunier, T. Bege, and C. Masson, "Assessment of the smartpill, a wireless sensor, as a measurement tool for intra-abdominal pressure (IAP)," *Sensors*, vol. 24, no. 1, p. 54, Dec. 2023.

[12] B. Kuo et al., "The assessment of gastrointestinal transit by the atmo capsule: A comparison with the SmartPill capsule," *Clin. Gastroenterology Hepatology*, vol. 23, no. 9, pp. 1633–1641, Aug. 2025.

[13] S. Gopalakrishnan et al., "Smart capsule for monitoring inflammation profile throughout the gastrointestinal tract," *Biosensors Bioelectronics, X*, vol. 14, Sep. 2023, Art. no. 100380.

[14] M. E. Inda-Webb et al., "Sub-1.4 cm3 capsule for detecting labile inflammatory biomarkers in situ," *Nature*, vol. 620, no. 7973, pp. 386–392, Aug. 2023.

[15] J. Min et al., "Continuous biochemical profiling of the gastrointestinal tract using an integrated smart capsule," *Nature Electron.*, vol. 8, no. 9, pp. 844–855, Jun. 2025.

[16] S.-Y. Yang et al., "A fully-integrated wireless ingestible drug delivery chip with electrochemical energy harvesting and pH-based MPPT," in *Proc. IEEE Custom Integr. Circuits Conf. (CICC)*, Apr. 2025.

[17] A. Even et al., "Measurements of redox balance along the gut using a miniaturized ingestible sensor," *Nature Electron.*, vol. 8, no. 9, pp. 856–870, Jul. 2025.

[18] Q. Lin et al., "A multichannel electrochemical sensor interface IC for bioreactor monitoring," *IEEE Trans. Biomed. Circuits Syst.*, vol. 17, no. 6, pp. 1227–1236, Dec. 2023.

[19] Q. Lin et al., "21.2 A 22μ W peak power multimodal electrochemical sensor interface IC for bioreactor monitoring," in *IEEE Int. Solid-State Circuits Conf. (ISSCC) Dig. Tech. Papers*, Feb. 2023.

[20] R. Jarmin, K. Y. Lee, S. M. Esa, H. Hashim, A. M. Sih, and M. A. Ghani, "ISFET characterization using constant voltage constant current readout circuit," *Int. J. Circuits, Syst. Signal Process.*, vol. 9, pp. 47–53, 2015.

[21] N. Ziebart, A. Gießel, and T. Walther, "The performance of commercial pH-sensitive ion-selective field effect transistors," *ChemistryOpen*, vol. 14, no. 12, Dec. 2025, Art. no. 202500361.

[22] L. J. Henze et al., "Characterization of gastrointestinal transit and luminal conditions in pigs using a telemetric motility capsule," *Eur. J. Pharmaceutical Sci.*, vol. 156, Jan. 2021, Art. no. 105627.

[23] H. A. Merchant et al., "Assessment of gastrointestinal pH, fluid and lymphoid tissue in the Guinea pig, rabbit and pig, and implications for their use in drug development," *Eur. J. Pharmaceutical Sci.*, vol. 42, nos. 1–2, pp. 3–10, Jan. 2011.

[24] S. Sharma, H. Melton, L. B. Edmonds, O. Addington, M. G. Shapiro, and A. Emami, "A 14.8-μW power and $<$10-μ trms noise 3-D AC magnetic sensor in CMOS for biomedical applications," *IEEE J. Solid-State Circuits*, vol. 60, no. 6, pp. 2072–2083, Jun. 2025.

[25] K. Yang et al., "9.2 A 0.6nJ -0.22/+0.19°C inaccuracy temperature sensor using exponential subthreshold oscillation dependence," in *IEEE Int. Solid-State Circuits Conf. (ISSCC) Dig. Tech. Papers*, Feb. 2017.

[26] P. A. Thwaites et al., "Review article: Current status and future directions of ingestible electronic devices in gastroenterology," *Alimentary Pharmacol. Therapeutics*, vol. 59, no. 4, pp. 459–474, Feb. 2024.

[27] S. Sharma et al., "Location-aware ingestible microdevices for wireless monitoring of gastrointestinal dynamics," *Nature Electron.*, vol. 6, no. 3, pp. 242–256, Feb. 2023.

[28] I. Castro, J. W. de Wit, J. van Vooren, T. Van Quaethem, W. Huang, and T. Torfs, "Magnetic localization of wireless ingestible capsules using a belt-shaped array transmitter," *Electronics*, vol. 12, no. 10, p. 2217, May 2023.

[29] M. Rehan, I. Al-Bahadly, D. G. Thomas, W. Young, L. K. Cheng, and E. Avci, "Smart capsules for sensing and sampling the gut: Status, challenges and prospects," *Gut*, vol. 73, no. 1, pp. 186–202, Jan. 2024.